Journal of Alloys and Compounds 1013 (2025) 178628

Contents lists available at ScienceDirect

Journal of Alloys and Compounds

journal homepage: www.elsevier.com/locate/jalcom

Fabrication and testing of ceramic thermoelectric multi-leg module for high-temperature energy conversion

P. Amirkhizi [a,*], M. Hedayati [a], M.A. Madre [b], O.J. Dura [c], M.A. Torres [b], A. Sotelo [b], A.V. Kovalevsky [a], Sh. Rasekh [a]

[a] Department of Materials and Ceramic Engineering, CICECO-Aveiro Institute of Materials, University of Aveiro, Aveiro 3810-193, Portugal
[b] INMA (CSIC-Universidad de Zaragoza), Mª de Luna, 3, Zaragoza 50018, Spain
[c] Applied Physics Department, University of Castilla-La Mancha , Ciudad Real 13071, Spain

ARTICLE INFO

Keywords:
Thermoelectric module
Power density
Thermoelectric properties
Oxides
Stability

ABSTRACT

This study investigates the fabrication and performance of ceramic-based thermoelectric modules for high-temperature energy conversion, based on $Ca_{2.93}Sr_{0.07}Co_4O_9$ and $Ca_{0.91}Y_{0.03}La_{0.03}Yb_{0.03}MnO_3$ p- and n-type materials. The p-type materials were prepared through attrition milling and classical sintering, while ball milling and hot uniaxial pressing were used for the n-type legs. The power factor reached 0.62 mW/(K^2m) for the p-type and 0.33 mW/(K^2m) for the n-type materials at 800 °C, being comparable to some of the best-reported values in literature. The lower thermal conductivity of n-type material (1.24 W/K/m) compared to the p-type material (1.56 W/K/m) resulted in similar ZT values for n-type (0.29) and p-type (0.43). The thermal expansion behaviour of the materials was also evaluated, demonstrating good thermal compatibility between the p- and n-type legs. The module's performance was tested at hot-side temperatures up to 900 °C, yielding a power density of 34 W/m^2. Moreover, the module demonstrated an energy conversion efficiency of 0.8 % (actual) and 6 % (theoretical), thereby underscoring the practical potential of these materials. Additionally, the module exhibited excellent long-term thermal stability, maintaining its performance after 2000 h of exposure at 900 °C and after undergoing 100 thermal cycles, demonstrating its suitability for high-temperature energy recovery applications.

1. Introduction

The rapid growth of the global population has drastically increased energy demand. However, traditional energy sources are finite and significantly contribute to global warming through greenhouse gas emissions. Energy conversion processes are often inefficient, with more than half of the initial energy typically lost as waste heat. This inefficiency underscores the importance of seeking alternative conversion processes, including those which allow recovery of waste heat [1–3].

One promising solution for energy recovery is thermoelectric generators (TEGs), devices designed for generating electrical power from heat flux. They incorporate a set of thermoelectric modules (TEMs). The use of TEGs, as waste heat harvesting devices, offers several advantages over other systems, such as turbomachines and systems based on thermodynamic cycles. These benefits include the absence of moving parts, compact design, and reasonable power output performance [4,5]. The efficiency of TEGs is largely determined by the power output of the TEMs, which consist of several thermoelectric (TE) semiconducting pairs, and by the system design, which governs the rate of heat transfer from the heat source to the TEMs.

Historically, the use of TEGs has been restricted due to the low energy conversion efficiencies of TE materials. However, with recent advancements in material science and module fabrication techniques, the conversion efficiency of TE materials has been improved, leading to enhanced power outputs for TEGs as reported by various research groups [6,7].

TEMs exploit the Seebeck effect for power generation and the Peltier effect for refrigeration, presenting a versatile solution for a wide range of industries, from renewable energy to electronic cooling systems. The efficiency and performance of TEMs depend heavily on the materials used and the precision of the fabrication process. Fabricating high-performance TEMs involves several critical steps, including material selection, processing of TE elements, and the assembly of these elements into a functional module. TEMs consist of pairs of p- and n-type semiconductor materials arranged electrically in series and thermally in parallel and sandwiched between two plates with suitable thermal

* Corresponding author.
E-mail address: parisa.amirkhizi@ua.pt (P. Amirkhizi).

https://doi.org/10.1016/j.jallcom.2025.178628
Received 13 November 2024; Received in revised form 4 January 2025; Accepted 11 January 2025
Available online 11 January 2025

conductivity [6–8].

Ceramic oxides offer several advantages for TEMs, enhancing the applicability of TE technology. These materials exhibit high chemical stability at elevated temperatures without degradation even under air or oxidizing atmospheres, ensuring the long-term operation and reliability even in harsh environments [9]. Traditional thermoelectric materials, such as Bi_2Te_3 and PbTe, while being efficient at lower temperatures, face challenges such as environmental concerns, high costs, and limited thermal stability at higher temperatures. By taking advantage of the unique properties of ceramic materials, TEMs can not only address the environmental and thermal stability challenges associated with traditional TEMs but also expand the range of possible applications, making them viable candidates for more sustainable and efficient energy solutions [9].

In addition to material selection and design, the assembly process, which includes the precise placement and bonding of TE elements onto substrates and electrical interconnects, is equally important to ensure minimal electrical contact resistance and effective thermal conductivity. However, there is still a shortage of available ceramic-based TEMs for practical uses and research on TEG design [10].

In this paper, two ceramic-based TEMs were fabricated employing $Ca_{2.93}Sr_{0.07}Co_4O_9$ and $Ca_{0.91}Y_{0.03}La_{0.03}Yb_{0.03}MnO_3$ as p- and n-type legs, respectively. The work focuses on the fabrication of TE modules, exploring advancements in materials science and engineering techniques that have paved the way for improved module performance. Power generation from the fabricated modules has been evaluated using a home-made system. One of the modules has been characterized after a different number of heating-cooling cycles (up to 100), and another after maintaining at 900 °C up to 2000 h, to evaluate its durability.

2. Materials and methods

A 17 p-n thermocouples TEM was fabricated using $Ca_{2.93}Sr_{0.07}Co_4O_9$ and $Ca_{0.91}Y_{0.03}La_{0.03}Yb_{0.03}MnO_3$ ceramic materials, which were selected due to their promising TE properties and compatible thermal expansion. The $Ca_{2.93}Sr_{0.07}Co_4O_9$ samples (p-type) were synthesized by combining appropriate amounts of $CaCO_3$ (≥ 99 %, Aldrich), $SrCO_3$ (≥ 98 %, Aldrich), and CoO (99.99 %, Aldrich) powders, which were attrition milled at 600 rpm for 1 hour, in distilled water media, using zirconia balls (∅ = 1 mm). The starting $Ca_{0.91}Y_{0.03}La_{0.03}Yb_{0.03}MnO_3$ mixtures (n-type) were prepared using commercially available $CaCO_3$ (≥99 %, Aldrich), Y_2O_3 (99.99 %, Aldrich), La_2O_3 (≥ 99.9 %, Aldrich), Yb_2O_3 (99.9 %, Aldrich) and Mn_2O_3 (99.9 %, Aldrich) powders, which were weighed in the appropriate proportions, mixed and ball milled for 30 minutes at 300 rpm in distilled water media. In both cases, the water-based suspensions were dried under IR radiation to obtain a very fine powder. Then, both samples were calcined for 1 h at 850 °C for the p-type samples and 950 and 1050 °C for 12 h for the n-type samples. Finally, n-type samples were cold-uniaxially pressed in the form of pellets (~ 3x3x18 mm^3) under 400 MPa and sintered at 1310 °C for 12 h, while p-type ones were cold-uniaxially pressed into disk-shaped pellets (25 mm in diameter and ~ 3.5 mm thick) under 250 MPa, followed by hot-uniaxial pressing at 900 °C and 55 MPa for 1 h. Finally, they were polished and cut with the same length as n-type samples.

Electrical resistivity (ρ) and the Seebeck coefficient (S) were measured simultaneously using the standard DC four-probe method on an LSR-3 system (Linseis GmbH) between 50 and 800 °C, with a heating rate of 10 °C/min under helium atmosphere for all sintered legs. Additionally, the power factor ($PF=S^2/\rho$) was calculated using the electrical resistivity and Seebeck coefficient data to assess their TE performance. The thermal diffusivity (α) has been measured for both samples using a laser-flash system (Linseis LFA 1000). The thermal conductivity (κ) was calculated using the equation $\kappa = \alpha \cdot c_p \cdot \rho$, where c_p represents the specific heat, calculated using the Dulong-Petit law, and ρ is the density of the sample. The thermoelectric performance of the samples (ZT) has then been calculated using the power factor and the thermal conductivity data.

Finally, the thermal expansion coefficient of both legs was evaluated during heating at a rate of 10 °C /min up to 850 °C in air, using a horizontal dilatometer (Linseis L79 HCS).

Once all legs were prepared, (~ 2 × 3 × 15 mm^3 after sintering or cutting) (Fig. 1), the resistance of each leg was measured at room temperature using the standard DC four-point probe method.

To establish electrical connections, an electric circuit was designed on two alumina plates, (5 × 5 cm^2) as the top and bottom substrates of the module, using silver conductive ink (Alfa Aesar), as shown in Fig. 2. Alumina plates were used considering their insulating properties and relatively high thermal conductivity. The ends of the legs were also coated with Ag ink and left to dry for 24 h. All legs and alumina plates were subsequently sintered in a furnace, first heated up to 450 °C at a rate of 1 °C/min with a dwell time of 1 h, then heated up to 900 °C at 5 °C/min for 4 hours, followed by furnace cooling. Subsequently, the n-type and p-type legs were alternately positioned on the alumina plate according to the module pattern (Fig. 3) and bonded using Ag adhesive conducting paste (Alfa Aesar). The assembled module was allowed to dry for 24 hours at 50 °C in an oven, followed by sintering at 900 °C for 4 h. Next, the opposite ends of the legs were painted with Ag paste. The second alumina plate was carefully placed on top of the legs, as shown in Fig. 4. Two Ag wires, each 200 mm in length, were attached to the beginning and the end of the circuit using Ag paste. The assembly was then allowed to dry, followed by sintering at 900 °C for 4 h under the same conditions used before.

The finally assembled module is shown in Fig. 5. A quick functional test was conducted to verify its proper operation before further characterization. Also, the resistance of the fabricated module was measured to calculate the manufacturing factor (MF) [11], using Eq. (1).

$$MF = \frac{total\ resistance\ of\ all\ legs}{resistance\ of\ the\ module} \times 100 \quad (1)$$

For characterization, the module was placed on a cooling surface maintained at approximately 16°C with flowing water, while the top surface was heated to temperatures ranging from 200 to 900 °C with 50 °C increments. The heating rate was set at 10 °C/min with a dwell time of 600 seconds at each temperature step to ensure thermal equilibration. During the test, a current ranging from 0 mA to the maximum, with increments of 1 mA, was applied to assess the module's electrical response under varying thermal conditions. Once maximum output power is obtained for each temperature, the energy conversion efficiency of the module at that temperature was calculated following Eq. (2)

$$\eta = \frac{P_{output}}{Q_{input}} \quad (2)$$

where P_{output} is the power experimentally obtained and Q_{input} is total heat transferred to the thermoelectric module and estimated using Eq. (3)

$$Q_{input} = Q_{Conductive} + Q_{Peltier} + Q_{Joule} \quad (3)$$

where, heat input at the hot side was determined using the total heat flow through the thermoelectric legs. This includes contributions from conductive heat ($Q_{conductive}$) transfer, Peltier heat $Q_{peltier}$ transfer, and Joule heating Q_{Joule}.

Conductive Heat Transfer is calculated using Fourier's law Eq. (4):

$$Q_{Conductive} = n \times k_{average} \times \Delta T \times A/L \quad (4)$$

where, n is the number of legs, 34, $\kappa_{average}$: Average thermal conductivity of the thermoelectric legs, A is cross-sectional area of each leg, L is height of each leg, and ΔT is the temperature gradient across the legs.

Peltier heat transfer is derived from the Seebeck effect: Eq. (5)

$$Q_{Peltier} = n \times S_{average} \times I \times T_{average} \quad (5)$$

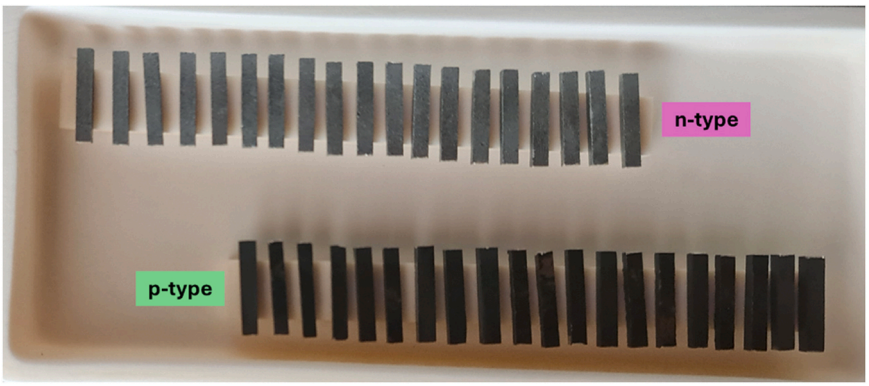

Fig. 1. The prepared n-type and p-type legs.

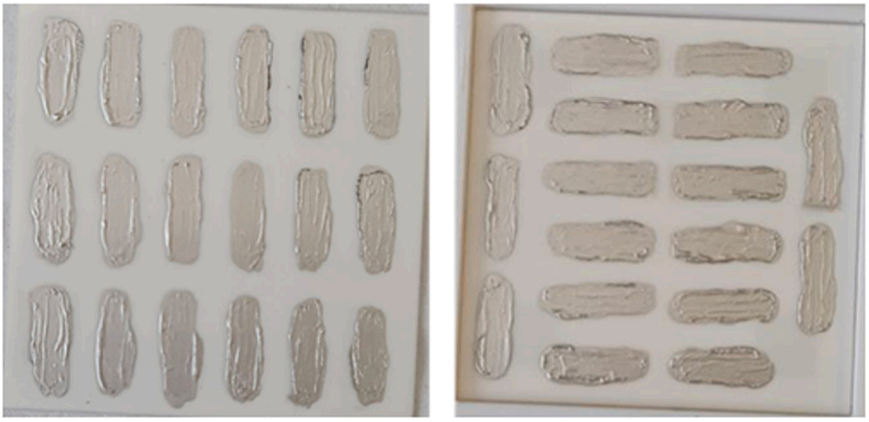

Fig. 2. Alumina plates with a circuit designed using Ag conductive ink.

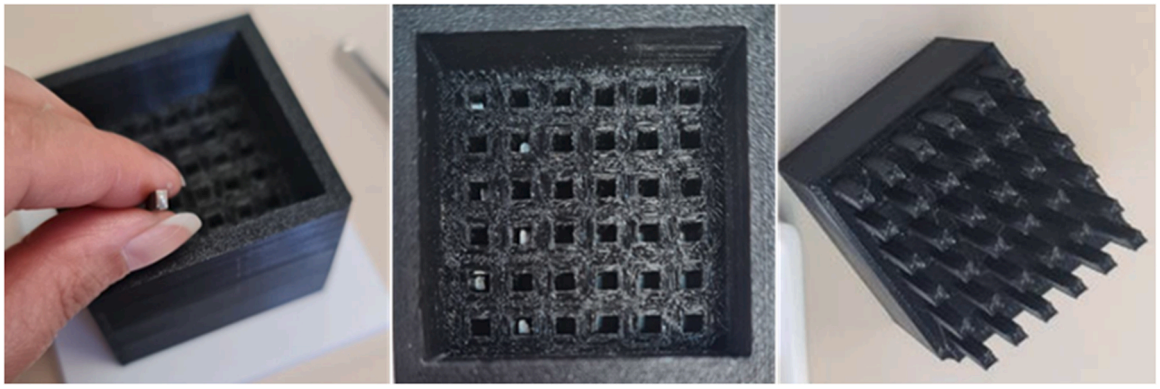

Fig. 3. Module assembly procedure.

where,

$$S_{average} = \frac{S_p - S_n}{2} \tag{6}$$

and

$$T_{average} = \frac{T_{hot} - T_{cold}}{2} \tag{7}$$

Joule heating, can be calculated using the total resistance of the module (R_{module}) previously determined, as

$$Q_{Joule} = I^2 \times R_{module} \tag{8}$$

Therefore, the actual energy conversion efficiency can be determined as

$$\eta_{actual} = \frac{P_{output}}{Q_{input}} \times 100 \quad \text{Eq. 9}$$

Additionally, the theoretical maximum efficiency for each temperature can be calculated using:

$$\eta_{max} = \frac{\Delta T}{T_{hot}} \times \left[\frac{\sqrt{1 + ZT_{average}} - 1}{\sqrt{1 + ZT_{average}} + \frac{T_C}{T_H}} \right] \times 100 \tag{10}$$

where $ZT_{average}$ is the average thermoelectric figure of merit for the module and is:

Fig. 4. Positioning the top plate according to the electrical configuration in series.

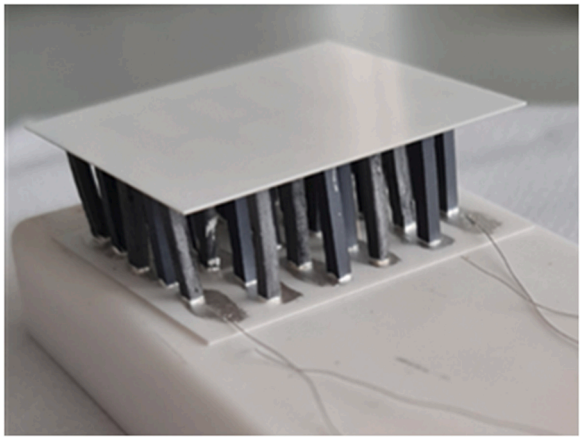

Fig. 5. Assembled thermoelectric module.

$$ZT_{average} = \frac{ZT_p + ZT_n}{2} \quad (11)$$

where ZT_p and ZT_n are the Figure of merit values for the p- and n-type materials, respectively.

The thermal cycling test included 100 heating and cooling cycles for the module, each cycle maintaining specified ramp rates and dwell times to mimic real-world operating conditions. In addition, a long-term stability test was conducted by holding the module at a constant temperature of 900 °C for 1000, and 2000 h, to evaluate its resistance to degradation and stability during prolonged exposure to high temperatures.

3. Results and discussions

As the first step, the legs were characterized in order to determine the relevant electrical properties of each material. The variation of electrical resistivity with temperature for both compounds, as shown in Fig. 6, reveals distinct behaviours for the n- and p-type TE materials. The p-type samples exhibited semiconducting-like behaviour above 100 °C, while the n-type compound showed metallic-like behaviour between 100 °C and 350 °C, transitioning to semiconducting-like behaviour above 350 °C. However, in general, the temperature dependence of the resistivity in the n-type samples is weak. At 800°C, the resistivity values were about 6.5 mΩ·cm for the p-type leg and 5.8 mΩ·cm for the n-type one. Both resistivity values are comparable to some of the best-reported values in the literature for both types of material families [12–20].

The variation of the Seebeck coefficient with temperature, as illustrated in Fig. 7, shows the expected behaviour for both p-type and n-type compounds. The p-type material displays positive Seebeck values, while the n-type material exhibits negative values, consistent with their

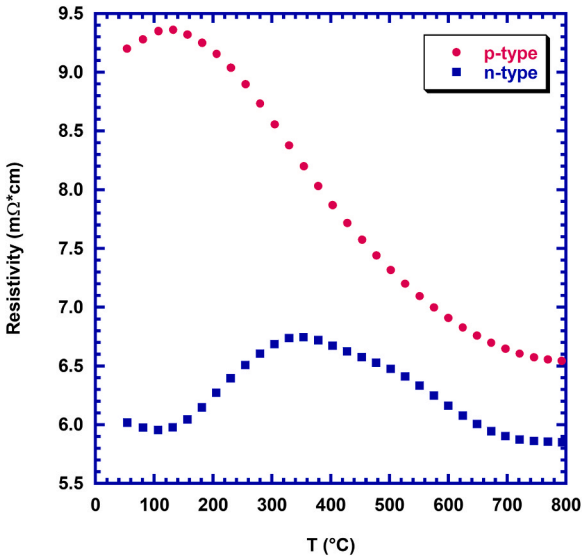

Fig. 6. Variation of electrical resistivity as a function of temperature for the prepared p- and n-type materials.

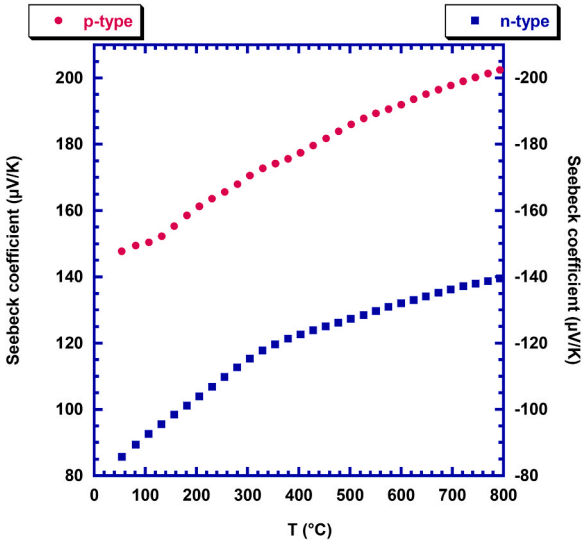

Fig. 7. Seebeck coefficient values as a function of temperature for both compounds.

respective charge carrier types (holes and electrons, respectively). For both materials, the absolute value of the Seebeck coefficient ($|S|$) increases steadily as the temperature rises, reaching about 200 μV/K for the p-type composition and 140 μV/K for the n-type one at 800 °C. This increasing trend indicates enhanced thermoelectric performance at higher temperatures, a critical factor for high-temperature applications. Nonetheless, these Seebeck coefficient values are well-aligned with those reported in the literature for similar thermoelectric materials, demonstrating the relevant thermoelectric performance of both compositions [12,13,21,22–24].

The thermoelectric performance of the samples was evaluated by calculating their power factor (*PF*), and presented, as a function of temperature, in Fig. 8. The graph shows a clear upward trend in *PF* for both the p- and n-type samples as the temperature increases. At 800 °C, the p-type compound achieved a maximum *PF* value of 0.62 mW/K^{2}m, while the n-type compound reached 0.33 mW/K^{2}m. These values are comparable to some of the best results reported in the literature, demonstrating the overall high electrical performance of both materials [22,24–28].

Fig. 9 depicts the variation of electronic, lattice and total thermal conductivity (κ_{el}, κ_{ph} and κ_{total}, respectively) with temperature for p- and n-type materials. As shown in Fig. 9a, the electronic thermal conductivity increases with temperature for both samples, which aligns with the previously discussed reduction in electrical resistivity. In contrast, the lattice contribution to thermal conductivity decreases with increasing temperature, reflecting enhanced phonon scattering. Consequently, as observed in Fig. 9b, the total thermal conductivity decreases on heating up to approximately 600 °C, particularly for the p-type material. This reduction is attributed to the increased phonon scattering caused by the increase of lattice vibrations. However, at higher temperatures, the total thermal conductivity begins to increase due to the greater contribution from the electronic counterpart. At 800 °C, the thermal conductivity is approximately 1.56 W/K/m for p-type material and 1.24 W/K/m for n-type one. These values rank among the lowest reported in the literature for both compounds highlighting their potential for thermoelectric applications [22,24,27].

Fig. 10 shows the evolution of the dimensionless figure of merit with temperature for both the p- and n-type samples, calculated from their electrical resistivity, Seebeck coefficient and thermal conductivity data. Interestingly, both legs exhibit a similar trend as temperature increases, reaching the ZT value of 0.43 and 0.29 at 800 °C for p- and n-type samples, respectively. The improvement in ZT for the p-type material is likely due to a significant increase in the Seebeck coefficient and an

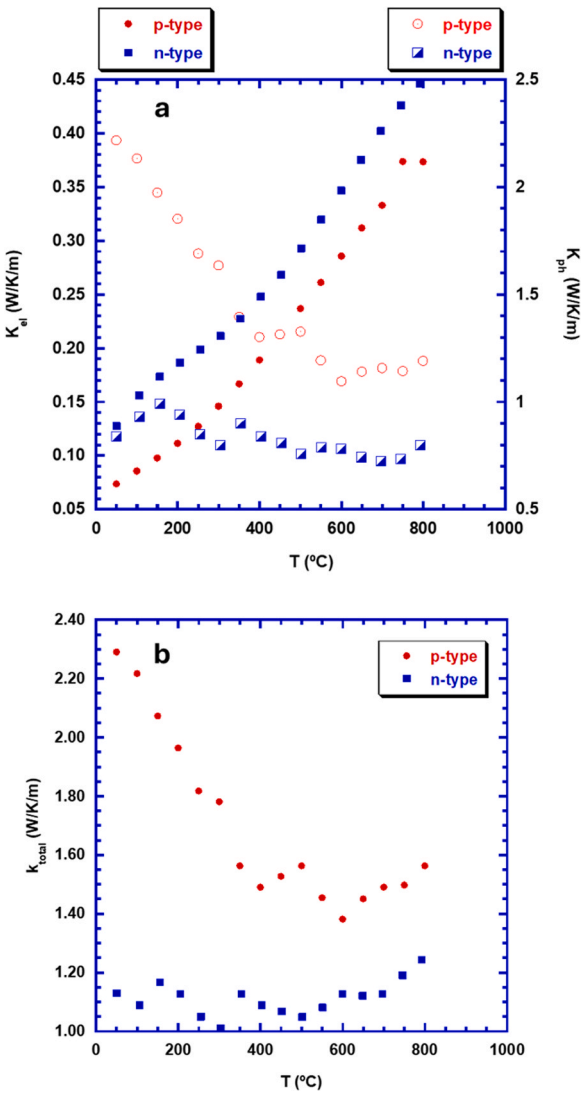

Fig. 9. Thermal conductivity values as a function of temperature for both compounds: (a) electronic; and lattice, (b) total thermal conductivity.

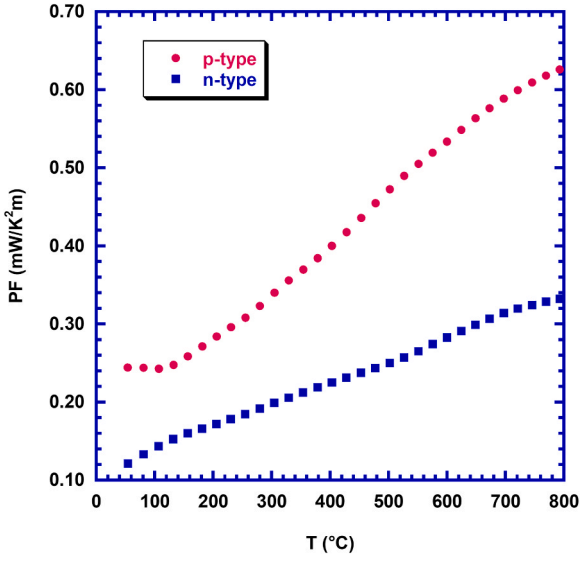

Fig. 8. Power factor values as a function of temperature for both compounds.

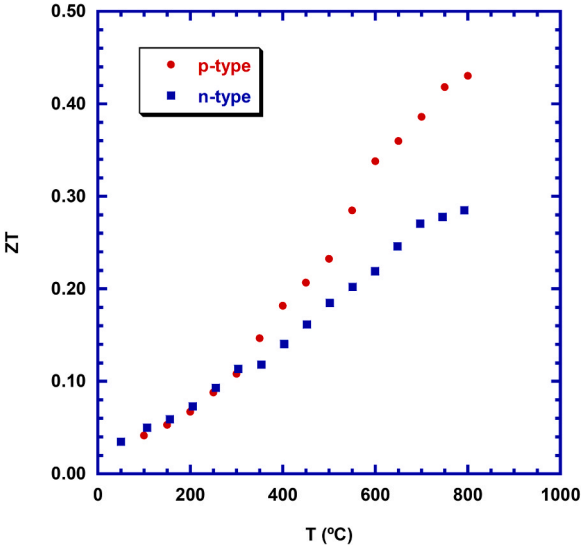

Fig. 10. ZT variation with temperature for both compounds.

enhanced power factor at high temperatures. For the n-type material, the ZT enhancement can be attributed to its low electrical resistivity and thermal conductivity. The combined effect of these factors results in comparable ZT values for both materials, making them a well-matched pair for thermoelectric module applications. It should be highlighted that these ZT values are among the highest reported in the literature, emphasizing the potential of these compounds for efficient thermoelectric performance [22,24,27,29].

Based on the dilatometry data, shown in Table 1, p-type and n-type samples exhibit comparable thermal expansion characteristics, again making them good candidates for pairing in a TE module. The p-type sample shows an overall expansion, with a change in length ($\Delta L = L_2 - L_1$) of 78.25 μm, while the n-type sample exhibits a ΔL of 74.78 μm during the heating from room temperature up to 850 °Cat a rate of 10 °C/min. The ΔL values and the coefficient of thermal expansion (CTEs) of both samples are closely aligned, suggesting that their thermal expansion behaviour is quite similar. The small difference in CTE values ($9.73 \cdot 10^{-6}$ K^{-1} for the p-type and $9.67 \cdot 10^{-6}$ K^{-1} for the n-type) indicates that both materials will expand and contract at nearly the same rate under varying temperature conditions, which is crucial for maintaining the mechanical integrity of a TE module. These values confirm very good compatibility of the selected materials, as compared to that of literature [30–32]. The close match between p-type and n-type in terms of both ΔL and CTE suggests that these two materials will expand uniformly when exposed to temperature gradients, thereby minimizing the risk of mechanical stresses at the interfaces between the TE legs and the electrical contacts. Furthermore, the similar slope values in the thermal expansion (0.203443 μm/°C for the p-type and 0.201724 μm/°C for the n-type) further reinforce the compatibility of these two materials. This matching ensures that the module will maintain its structural integrity under operating conditions, leading to improved durability and long-term performance.

After evaluating the properties of the different legs, they were assembled into two operational TE modules, as described in the experimental procedure. Firstly, the manufacturing factor for the prepared thermoelectric module was calculated based on the resistance of its legs. Given that the module contained 17 n-type and 17 p-type legs, the total resistance of the legs was approximately 3 Ω (2.55, and 0.51 Ω for the 17 p- and n-type samples, respectively). The total resistance of the module, as measured, was ca. 10 Ω. Using these values, the manufacturing factor was determined to be around 30 %, calculated following Eq. (1). This value, which represents good agreement with the previous reported results [33–35], reflects the effectiveness of the module's assembly procedure. It should be mentioned that both modules present approximately the same value. The evolution of power output with voltage at different hot-side temperatures is presented in Fig. 11. As the hot-side temperature increases, the power output rises accordingly, reaching about 85 mW (935 mV, 91 mA) at 900 °C with a temperature gradient of 555 °C indicating that higher temperatures result in more efficient energy conversion. This value is comparable with those presented in the literature and shows an improvement in comparison with some documented results [36–40]. Although the power output may seem low, it is important to consider the module's dimensions, 5 × 5 cm^2 (0.0025 m^2), which roughly corresponds to ~34 W/m^2 power density. This value is only ~6 times lower than the typical power density achieved by photovoltaic cells [41]. Moreover, the power output is negatively affected by the large spacing between the TE elements, due to the limited number of TE pairs used in this module design, as well as the relatively weak thermal contact of the module with the cold and hot sides of the measuring system. This weak thermal contact leads to 770 °C maximum temperatures on the hot side, and 215 °C minimum temperature on the cold side (when the hot side of the system reaches 900 °C), drastically decreasing the module conversion efficiency. As a consequence, the real output power values should be higher than those presented in this manuscript. However, despite all these negative factors, the results demonstrate the significant potential of the fabricated oxide-based thermoelectric modules for converting heat into electricity in high-temperature applications. These findings underscore the promise of thermoelectric devices in contributing to global energy sustainability efforts, particularly as improvements in design and material optimization continue to enhance their overall efficiency and power output.

Table 1
The ΔL values and CTEs of both samples.

Sample	ΔL (μm)	Average slope (μm/°C)	CTE (10^{-6} K^{-1})
p-type	*78.25*	*0.203443*	*9.73*
n-type	*74.78*	*0.201724*	*9.67*

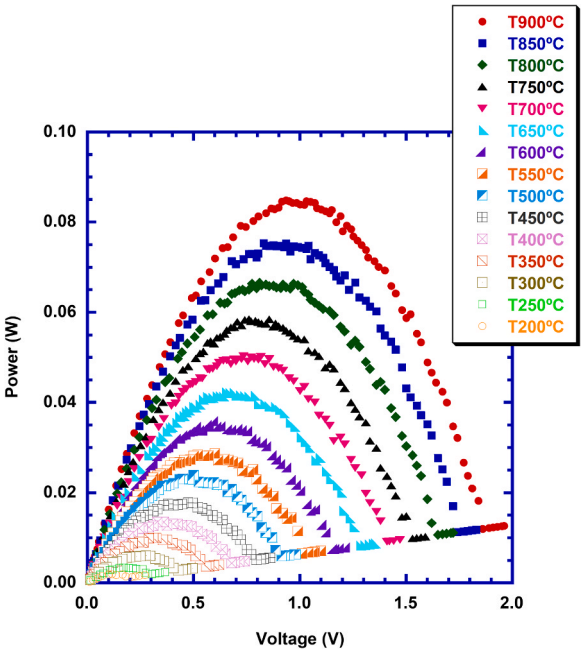

Fig. 11. Power vs. Voltage at different hot-side temperatures, with cold side temperature fixed at 16 °C.

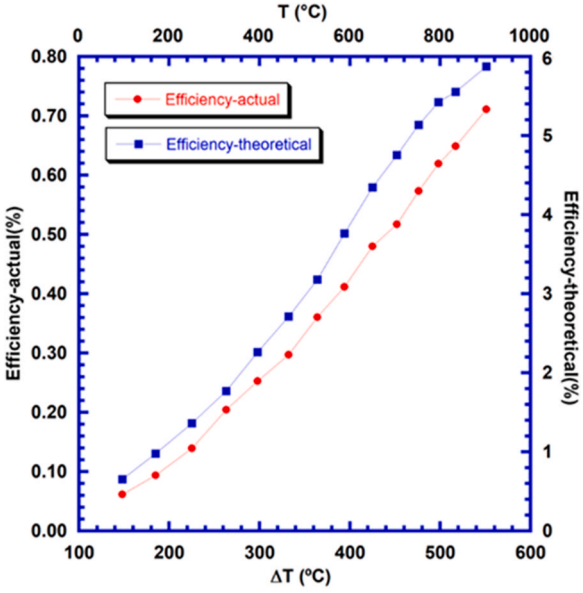

Fig. 12. Theoretical and actual energy conversion efficiencies as a function of temperature and temperature difference (ΔT).

The graph in Fig. 12 illustrates the evolution of both theoretical and actual energy conversion efficiencies as a function of the temperature (T) and temperature difference (ΔT) across the thermoelectric module.

In the graph an almost linear and significant increase with temperature difference (which is function of the hot side temperature) can be seen for both efficiencies, in agreement with the increase of power output of the module with temperature. This demonstrates a strong alignment between predicted and measured performance. Moreover, the consistent shape of the two curves across the whole range of ΔT suggests that the module design optimally balances the contributions of p-type and n-type legs. Furthermore, it can be seen that the actual efficiency values are around 10 % of the maximum one. This divergence highlights the growing influence of non-idealities at large temperature differences, including the limited thermal conductivity and electrical resistance of the materials. Despite these factors, the actual efficiency curve retains a similar shape to the theoretical trend, indicating that the module effectively harnesses the thermoelectric potential of its materials. This difference is mainly attributed to thermal and electrical losses produced from Joule Heating, low module manufacturing factor (30 %), space between the legs, heat transfer to the environment, etc.

Nevertheless, to the knowledge of the authors no efficiency values have been reported for ceramic-based thermoelectric modules specifically at high temperature, namely 900°C. Moreover, the theoretical values, obtained from measured thermoelectric properties of these materials, clearly indicate the potential of these modules for high temperature applications, once fabrication process is optimized. These values are comparable with reported data for modules with intermediate working temperature such as Skutterudite-based [42] or PbTe-based ones [43] where thermal heat transfer is much lower.

Long-term stability test was conducted for one of the modules at 900 °C for up to 2000 h, and the power output was compared to that of the as-processed module and presented in Fig. 13. The data obtained from as-processed, and after 1000 and 2000 h at 900 °C, indicate that the module exhibits nearly identical power output curves, demonstrating its remarkable stability and reliability over time, even subjected at high temperatures. The peak power output occurs at approximately the same voltage value for all cases, being slightly higher after thermal treatment, (1.1 V and 80 mA). These results indicate exceptional thermal stability in the high-temperature working regime, unlike many other TE materials that suffer degradation, oxidation, or increased resistance after extended periods at high temperatures under air. The lack of any noticeable change in peak power output or the overall shape of the power curve suggests that the module's material composition and structural integrity remain intact, even after 2000 h at 900 °C. This result also indicates that no significant degradation, drastic microstructural changes affecting the legs performances, or increased contact resistance, occurred during the long-term test.

Another important parameter to take into account is that these modules can be subjected to cyclic heating-cooling processes. Consequently, the second module was further evaluated through thermal cycling, where the module underwent 100 heating-cooling cycles. The power output variation with voltage for each cycle is shown in Fig. 14. As evidenced by the overlapping curves across all cycles, there is no significant change in the power output throughout the cycling process, again suggesting excellent thermal stability and durability of the module. From cycle 1 to cycle 100, the power output curves remain almost the same, with the peak power output occurring at approximately the same voltage value across all cycles. The stability in both the peak power and the overall curve shapes demonstrates that the TE module's performance is unaffected by repeated thermal cycling, highlighting the ability of the module to maintain its efficiency even under cyclic thermal stresses. The lack of any visible shifts or reductions in power output over these 100 cycles suggests that the module is highly resistant to common degradation mechanisms of this type of devices, such as microcracking, delamination, or increasing contact resistance, which often affect TE materials subjected to repetitive thermal cycling. The durability displayed in these results indicates that the module is well-suited for long-term applications that involve continuous temperature changes. The module's ability to maintain stable performance after 100 thermal cycles is highly promising for real-world applications where devices experience regular temperature fluctuations, such as in waste heat recovery systems or high-temperature power generation.

4. Conclusions

In this study, two thermoelectric modules were fabricated using ceramic-based materials, specifically $Ca_{2.93}Sr_{0.07}Co_4O_9$ as the p-type, and $Ca_{0.91}Y_{0.03}La_{0.03}Yb_{0.03}MnO_3$ as the n-type legs. The successful synthesis, assembly, and characterization of the modules demonstrate the significant potential of ceramic oxide thermoelectric materials for high-

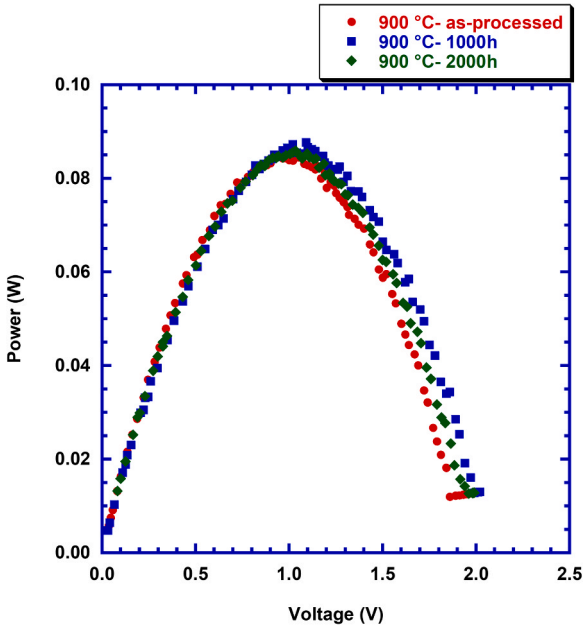

Fig. 13. Long-term stability of module up to 2000 h.

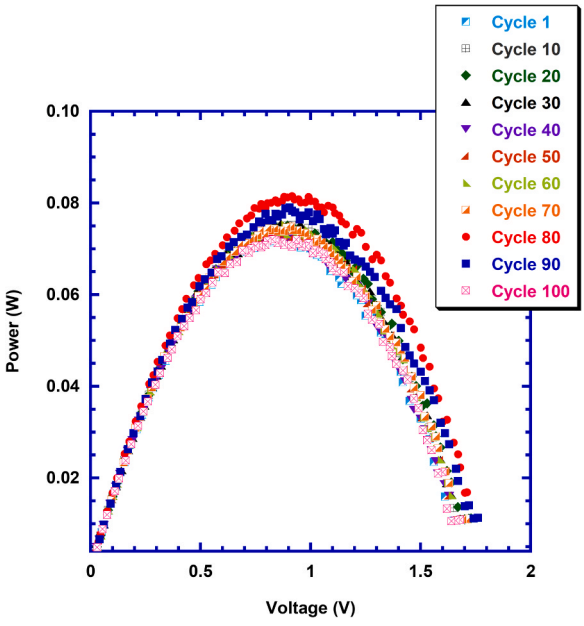

Fig. 14. Variation of power values as a function of voltage in 100 heating-cooling cycles. The curves have been recorded on heating.

temperature applications. Both materials exhibited excellent thermoelectric properties, with power factors of 0.62 mW/K^{2}m for the p-type and 0.33 mW/K^{2}m for the n-type at 800 °C, comparable to leading values in the literature. The lower thermal conductivity of the n-type material (1.24 W/K/m) compared to the p-type one (1.56 W/K/m) results in nearly identical ZT values for the n- (0.29) and p-type (0.43) materials, resulting in power output of ca. 85 mW (935 mV, 91 mA) with a temperature gradient of 555 °C. Moreover, energy conversion efficiency shows actual values of 0.8 % and theoretical value of 6 %, comparable with commercial intermetallic module at moderate temperature of around 550 °C, which highlighting the potential of these materials for practical application. The similar thermal expansion behaviour of the two compositions further reinforced their compatibility, ensuring the mechanical stability and integrity of the module. The modules were subjected to extensive performance tests, including operation at temperatures up to 900°C, during 100 thermal cycles, and long-term stability testing for up to 2000 h at 900 °C. Throughout these tests, the modules maintained consistent power output and exhibited remarkable durability, underscoring the thermal and structural stability of the selected materials. These results highlight the viability of oxide-based thermoelectric modules for waste heat recovery and energy generation in extreme environments, providing a reliable and efficient solution for sustainable energy applications. Future work should focus on optimizing the design and reducing the internal resistances to further enhance the power density and overall performance of these modules, as well as improving the thermal contact between the thermoelectric module and the measuring system to obtain values closer to the real ones.

CRediT authorship contribution statement

A. Sotelo: Writing – review & editing, Writing – original draft, Validation, Supervision, Resources, Project administration, Conceptualization. **A.V. Kovalevsky:** Writing – review & editing, Supervision, Funding acquisition, Conceptualization. **M.A. Torres:** Software, Formal analysis, Data curation. **M. Hedayati:** Writing – review & editing, Methodology. **M.A. Madre:** Validation, Software, Formal analysis, Data curation. **Parisa Amirkhizi:** Writing – review & editing, Writing – original draft, Methodology, Investigation, Formal analysis. **O.J. Dura:** Data curation, Formal analysis, Investigation, Software. **Sh. Rasekh:** Writing – review & editing, Supervision, Funding acquisition, Conceptualization.

Declaration of Competing Interest

The authors declare that they have no known competing financial interests or personal relationships that could have appeared to influence the work reported in this paper.

Acknowledgements

The authors wish to thank the Gobierno de Aragón, Spain (Grupo de Investigacion T54_23R) for financial support. Sh. Rasekh acknowledges the support of the Research Employment Contract FCT–CEECIND/02608/2017. This work was also developed within the scope of the Ph. D. project of P. Amirkhizi (grant 2020.08051.BD funded by FCT) and the project CICECO-Aveiro Institute of Materials, UIDB/50011/2020 (DOI 10.54499/UIDB/50011/2020), UIDP/50011/2020 (DOI 10.54499/UIDP/50011/2020) & LA/P/0006/2020 (DOI 10.54499/LA/P/0006/2020), financed by national funds through the FCT/MCTES (PIDDAC). Authors would like to acknowledge the use of Servicio General de Apoyo a la Investigación-SAI, Universidad de Zaragoza, Spain. This article was supported by the projects UIDB/00481/2020 and UIDP/00481/2020 - Fundação para a Ciência e a Tecnologia, DOI 10.54499/UIDB/00481/2020 (https://doi.org/10.54499/UIDB/00481/2020) and DOI 10.54499/UIDP/00481/2020 (https://doi.org/10.54499/UIDP/00481/2020). M. A. Madre, M. A. Torres, and A. Sotelo acknowledge the grant CEX2023–001286-S funded by MICIU/AEI /10.13039/501100011033. This article was also supported by the Ministerio de Ciencia, Innovación y Universidades (MICIU) /Agencia Estatal de Investigación (AEI), Spain.

Data availability

Data will be made available on request.

References

[1] D. Champier, Thermoelectric generators: a review of applications, Energy Convers. Manag 140 (2017) 167–181, https://doi.org/10.1016/j.enconman.2017.02.070.
[2] S. Twaha, J. Zhu, Y. Yan, B. Li, A comprehensive review of thermoelectric technology: materials, applications, modelling and performance improvement, Renew. Sustain. Energy Rev. 65 (2016) 698–726, https://doi.org/10.1016/j.rser.2016.07.034.
[3] H. Ohta, Thermoelectrics based on strontium titanate, Mater. Today 10 (2007) 44–49, https://doi.org/10.1016/S1369-7021(07)70244-4.
[4] A.Z. Sahin, B.S. Yilbas, The thermoelement as thermoelectric power generator: effect of leg geometry on the efficiency and power generation, ECM 65 (2013) 26–32, https://doi.org/10.1016/j.enconman.2012.07.020.
[5] W. Liu, Q. Jie, H.S. Kim, Z. Ren, ScienceDirect Current progress and future challenges in thermoelectric power generation: from materials to devices, Acta Mater. 87 (2015) 357–376, https://doi.org/10.1016/j.actamat.2014.12.042.
[6] M.A. Zoui, J.G. Stocholm, M. Bourouis, A review on thermoelectric Generators: progress and applications, Energies (2020), https://doi.org/10.3390/en13143606.
[7] M. d'Angelo, C. Galassi, N. Lecis, Thermoelectric materials and applications: a review, Energies 16 (2023) 6409, https://doi.org/10.3390/en16176409.
[8] D. Enescu, Thermoelectric energy harvesting: basic principles and applications, Green. Energy Adv. (2019), https://doi.org/10.5772/intechopen.83495.
[9] P. Zhang, Z. Lou, L. Gong, Z. Wu, X. Chen, W. Xu, Y. Wang, J. Xu, Z. Dashevsky, F. Gao, Development and applications of thermoelectric oxide ceramics and devices, Energies 16 (2023) 4475, https://doi.org/10.3390/en16114475.
[10] L. Catalan, O. Herrero, M. Araiz, A. Rodriguez, The importance of the assembly in thermoelectric generators, Generators (2018), https://doi.org/10.5772/intechopen.75697.
[11] D.M. Rowe, G. Min, Evaluation of thermoelectric modules for power generation, J. Power Sources 73 (1998) 193–198, https://doi.org/10.1016/S0378-7753(97)02801-2.
[12] M.A. Torres, F.M. Costa, D. Flahaut, K. Touati, S. Rasekh, N.M. Ferreira, J. Allouche, M. Depriester, M.A. Madre, A.V. Kovalevsky, J.C. Diez, A. Sotelo, Significant enhancement of the thermoelectric performance in $Ca_3Co_4O_9$ thermoelectric materials through combined strontium substitution and hot-pressing process, J. Eur. Ceram. Soc. 39 (2019) 1186–1192, https://doi.org/10.1016/j.jeurceramsoc.2018.12.049.
[13] X.L. Tang, Z.H. Ge, Z. Li, K. Zhao, Enhanced thermoelectric properties of $Ca_3Co_4O_{9+\delta}$ ceramics by Sr substitution, Solid State Sci. 104 (2020) 106190, https://doi.org/10.1016/j.solidstatesciences.2020.106190.
[14] A. Sotelo, G. Constantinescu, S. Rasekh, M.A. Torres, J.C. Diez, M.A. Madre, Improvement of thermoelectric properties of $Ca_3Co_4O_9$ using soft chemistry synthetic methods, J. Eur. Ceram. Soc. 32 (2012) 2415–2422, https://doi.org/10.1016/j.jeurceramsoc.2012.02.012.
[15] P. Amirkhizi, M.A. Torres, O.J. Dura, A. Sotelo, M.A. Madre, A. Kovalevsky, S. Rasekh, Effect of B-site doping on the thermoelectric performances of $Ca_{0.97}Y_{0.01}La_{0.01}Yb_{0.01}Mn_{1-2x}Nb_xMo_xO_3$ thermoelectric ceramics, J. Eur. Ceram. Soc. 44 (2024) 2982–2988, https://doi.org/10.1016/j.jeurceramsoc.2023.12.067.
[16] M. Gürsul, G. Çetin, Ergin, L. Korkmaz, B. Özçelik, M.A. Torres, M.A. Madre, A. Sotelo, Remarkable variation in microstructural, thermoelectric, and magnetic properties of $CaMnO_3$ through Ce doping, Mater. Sci. Eng.: B 299 (2024), https://doi.org/10.1016/j.mseb.2023.116986.
[17] A. Azulay, N. Caspin, D. Freidzon, Y. Kauffmann, H. Kleinke, Y. Amouyal, Y and La doping in $CaMnO_3$ compounds: effects of dopant identity and amount on charge transport kinetics, Adv. Energy Sustain. Res. (2023) 2300191, https://doi.org/10.1002/aesr.202300191.
[18] K.K. Liu, Z.Y. Liu, F.P. Zhang, J.X. Zhang, X.Y. Yang, J.W. Zhang, J.L. Shi, G. Ren, T.W. He, J.J. Duan, Improved thermoelectric performance in Pr and Sr Co-doped $CaMnO_3$ materials, J. Alloy. Compd. 808 (2019), https://doi.org/10.1016/j.jallcom.2019.07.188.
[19] C. Li, Q. Chen, Y. Yan, Effects of Pr and Yb dual doping on the thermoelectric properties of $CaMnO_3$, Materials 11 (2018) 1–13, https://doi.org/10.3390/ma11101807.
[20] M.A. Madre, H. Amaveda, O.J. Dura, D. Pelloquin, M. Mora, M.A. Torres, S. Marinel, A. Sotelo, Effect of Y, La, and Yb simultaneous doping on the thermal conductivity and thermoelectric performances of $CaMnO_3$ ceramics, J. Alloy. Compd. 954 (2023), https://doi.org/10.1016/j.jallcom.2023.170201.
[21] D. Flahaut, T. Mihara, R. Funahashi, N. Nabeshima, K. Lee, H. Ohta, K. Koumoto, Thermoelectrical properties of A -site substituted $Ca_{1-x}Re_xMnO_3$ system, J. Appl. Phys. 100 (2006), https://doi.org/10.1063/1.2362922.

[22] Y.H. Zhu, W. Bin Su, J. Liu, Y.C. Zhou, J. Li, X. Zhang, Y. Du, C.L. Wang, Effects of Dy and Yb co-doping on thermoelectric properties of $CaMnO_3$ ceramics, Ceram. Int 41 (2015) 1535–1539, https://doi.org/10.1016/j.ceramint.2014.09.089.
[23] P. Kumar, SubhashC. Kashyap, Vijay Kumar Sharma, H.C. Gupta, Improved thermoelectric property of cation-substituted $CaMnO_3$, Chin. Phys. B 24 (2015), https://doi.org/10.1088/1674-1056/24/9/098101.
[24] J. Yu, X. Liu, W. Xiong, B. Wang, M.J. Reece, R. Freer, The effects of dual-doping and fabrication route on the thermoelectric response of calcium cobaltite ceramics, J. Alloy. Compd. 902 (2022) 163819, https://doi.org/10.1016/j.jallcom.2022.163819.
[25] Y.C. Zhou, C.L. Wang, W.B. Su, J. Liu, H.C. Wang, J.C. Li, Y. Li, J.Z. Zhai, Y. C. Zhang, L.M. Mei, Electrical properties of Dy^{3+}/Na^{+}Co-doped oxide thermoelectric $[Ca_{1-x}(Na_{1/2}Dy_{1/2})_x]MnO_3$ ceramics, J. Alloy. Compd. 680 (2016) 129–132, https://doi.org/10.1016/j.jallcom.2016.04.158.
[26] N.M. Ferreira, N.R. Neves, M.C. Ferro, M.A. Torres, M.A. Madre, F.M. Costa, A. Sotelo, A.V. Kovalevsky, Growth rate effects on the thermoelectric performance of $CaMnO_3$-based ceramics, J. Eur. Ceram. Soc. 39 (2019) 4184–4188, https://doi.org/10.1016/j.jeurceramsoc.2019.06.011.
[27] D. Kenfaui, B. Lenoir, D. Chateigner, B. Ouladdiaf, M. Gomina, J.G. Noudem, Development of multilayer textured $Ca_3Co_4O_9$ materials for thermoelectric generators: Influence of the anisotropy on the transport properties, J. Eur. Ceram. Soc. 32 (2012) 2405–2414, https://doi.org/10.1016/j.jeurceramsoc.2012.03.022.
[28] G. Constantinescu, S. Rasekh, M.A. Torres, J.C. Diez, M.A. Madre, A. Sotelo, Effect of Sr substitution for Ca on the $Ca_3Co_4O_9$ thermoelectric properties, J. Alloy. Compd. 577 (2013) 511–515, https://doi.org/10.1016/j.jallcom.2013.07.005.
[29] R. Kabir, R. Tian, T. Zhang, R. Donelson, T.T. Tan, S. Li, "Role of Bi doping in thermoelectric properties of $CaMnO_3$, J. Alloy. Compd. 628 (2015) 347–351.
[30] Y. Gelbstein, J. Tunbridge, R. Dixon, M.J. Reece, H. Ning, R. Gilchrist, R. Summers, I. Agote, M.A. Lagos, K. Simpson, C. Rouaud, P. Feulner, S. Rivera, R. Torrecillas, M. Husband, J. Crossley, I. Robinson, Physical, mechanical, and structural properties of highly efficient nanostructured n-and p-silicides for practical thermoelectric applications, J. Electron Mater. 43 (2014) 1703–1711, https://doi.org/10.1007/s11664-013-2848-9.
[31] M. Mejri, Y. Thimont, B. Malard, C. Estournès, Characterization of the thermo-mechanical properties of p-type ($MnSi_{1.77}$) and n-type ($Mg_2Si_{0.6}Sn_{0.4}$) thermoelectric materials, Scr. Mater. 172 (2019) 28–32, https://doi.org/10.1016/j.scriptamat.2019.06.037.
[32] H. Ihou Mouko, K. Romanjek, M. Mejri, M. Oulfarsi, S. El Oualid, P. Malinconi, Y. Thimont, B. Malard, C. Estournès, N. David, A. Dauscher, Manufacturing and performances of silicide-based thermoelectric modules, Energy Convers. Manag. 242 (2021), https://doi.org/10.1016/j.enconman.2021.114304.
[33] E.S. Reddy, J.G. Noudem, S. Hebert, C. Goupil, Fabrication and properties of four-leg oxide thermoelectric modules, J. Phys. D Appl. Phys. 38 (2005) 3751–3755, https://doi.org/10.1088/0022-3727/38/19/026.
[34] J.G. Noudem, S. Lemonnier, M. Prevel, E.S. Reddy, E. Guilmeau, C. Goupil, Thermoelectric ceramics for generators, J. Eur. Ceram. Soc. 28 (2008) 41–48, https://doi.org/10.1016/j.jeurceramsoc.2007.05.012.
[35] H.S. Han, Y.H. Kim, S.Y. Kim, S. Um, J.M. Hyun, Performance measurement and analysis of a thermoelectric power generator, 12th IEEE Intersoc. Conf. Therm. Thermomech. Phenom. Electron. Syst. 2010 (2010) 1–7, https://doi.org/10.1109/ITHERM.2010.5501389.
[36] N.M. Ferreira, D. Lopes, A.V. Kovalevsky, F.M. Costa, A. Sotelo, M.A. Madre, A. Rezania, Thermoelectric modules built using ceramic legs grown by laser floating zone, Ceram. Int. 46 (2020) 24318–24325, https://doi.org/10.1016/j.ceramint.2020.06.213.
[37] S.F. Hayashi, T. Nakamura, K. Kageyama, H. Takagi, Monolithic thermoelectric devices prepared with multilayer cofired ceramics technology, Jpn. J. Appl. Phys. 49 (2010), https://doi.org/10.1143/JJAP.49.096505.
[38] O.V. Merkulov, B.V. Politov, K.Y. Chesnokov, A.A. Markov, I.A. Leonidov, M. V. Patrakeev, Fabrication and testing of a tubular thermoelectric module based on oxide elements, J. Electron Mater. 47 (2018) 2808–2816, https://doi.org/10.1007/s11664-018-6150-8.
[39] Z. Zhan, M. ElKabbash, Z. Li, X. Li, J. Zhang, J. Rutledge, S. Singh, C. Guo, Enhancing thermoelectric output power via radiative cooling with nanoporous alumina, Nano Energy 65 (2019) 104060, https://doi.org/10.1016/j.nanoen.2019.104060.
[40] S.M. Choi, K.H. Lee, C.H. Lim, W.S. Seo, Oxide-based thermoelectric power generation module using p-type $Ca_3Co_4O_9$ and n-type $(ZnO)_7In_2O_3$ legs, Energy Convers. Manag 52 (2011) 335–339, https://doi.org/10.1016/j.enconman.2010.07.005.
[41] M. Abdelhamid, Comparison of an analytical hierarchy process and fuzzy axiomatic design for selecting appropriate photovoltaic modules for onboard vehicle design, Int. J. Mod. Eng. 15 (1) (2014) 23–35, http://ijme.us/issues/fall2014/Z_IJME%20fall%202014%20v15%20n1%20(PDW-1).pdf.
[42] J.R. Salvador, J.Y. Cho, Z. Ye, J.E. Moczygemba, A.J. Thompson, J.W. Sharp, J. D. Koenig, R. Maloney, T. Thompson, J. Sakamoto, H. Wangf, A.A. Wereszczak, Conversion efficiency of skutterudite-based thermoelectric modules, Phys. Chem. Chem. Phys. 16 (24) (2014) 12510–12520, https://doi.org/10.1039/c4cp01582g.
[43] X. Hu, P. Jood, M. Ohta, M. Kunii, K. Nagase, H. Nishiate, M.G. Kanatzidisbc, A. Yamamoto, Power generation from nanostructured PbTe-based thermoelectrics: comprehensive development from materials to modules, Energy Environ. Sci. 9 (2016) 517–529, https://doi.org/10.1039/C5EE02979A.